Rugged mHz-Linewidth Superradiant Laser Driven by a Hot Atomic Beam

Haonan Liu,[1] Simon B. Jäger,[1] Xianquan Yu,[2] Steven Touzard,[2] Athreya Shankar,[1] Murray J. Holland,[1] and Travis L. Nicholson[2,*]

[1]JILA, National Institute of Standards and Technology, and University of Colorado, Boulder, Colorado 80309-0440, USA
[2]Centre for Quantum Technologies, Department of Physics, National University of Singapore, Singapore 117543

(Received 24 September 2020; accepted 19 November 2020; published 18 December 2020)

We propose a new type of superradiant laser based on a hot atomic beam traversing an optical cavity. We show that the theoretical minimum linewidth and maximum power are competitive with the best ultracoherent clock lasers. Also, our system operates naturally in continuous wave mode, which has been elusive for superradiant lasers so far. Unlike existing ultracoherent lasers, our design is simple and rugged. This makes it a candidate for the first widely accessible ultracoherent laser, as well as the first to realize sought-after applications of ultracoherent lasers in challenging environments.

DOI: 10.1103/PhysRevLett.125.253602

Ultracoherent light sources are the foundation of highly accurate atomic clocks [1,2], measurements of the time variation of fundamental constants [3,4], novel tests of relativity [5,6], and dark matter searches [7]. Traditionally, these sources have been generated with cavity stabilization, which involves locking lasers to highly stable optical cavities [8]. Despite their incredible performance [9], these systems are complex, challenging to improve upon, and perform poorly outside of controlled lab environments. However if cavity-stabilized lasers could be made rugged, they could be used for improved global positioning, deep space navigation [10], and new geophysical technology [11].

Superradiant lasers [12–21] are promising candidates for next-generation ultracoherent lasers [22]. However, a continuous wave superradiant laser has not yet been demonstrated because of atomic heating in existing designs, which rely on ultracold atoms [17]. Also, the use of ultracold atoms makes these systems complicated and ill suited to applications in the field.

Here we propose a new kind of superradiant laser built from a hot atomic beam traversing an optical cavity. We show that its theoretical minimum linewidth and maximum output power are competitive with the best ultracoherent lasers. Because of atomic phase synchronization, the phase of the output light is robust against decoherence arising from atomic motion, such as Doppler and transit time broadening. Furthermore, our system is naturally continuous wave, and it is inherently insensitive to effects that limit the best cavity-stabilized lasers [8,9], such as environmental noise and drift. The simplicity and ruggedness of the design make this system promising for applications in challenging real-world environments [6,23] and for packaging into commercial systems.

Our system consists of a dense atomic beam traveling through an optical cavity. We consider the case of all atoms having a uniform velocity in the x direction (Fig. 1). In this work, we discuss the examples of ^{40}Ca and ^{88}Sr, but our results apply equally well to many other alkaline-earth-like species. The mean intracavity atom number is $N \equiv \Phi\tau$ in steady state, where Φ is the number of atoms transiting the cavity mode per unit time, and τ is the transit time. The atoms in the beam are described by dipoles that are pumped into a metastable state (Fig. 1) before entering the cavity.

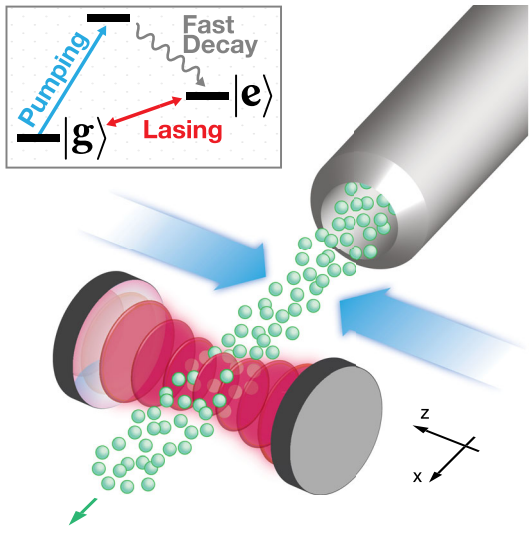

FIG. 1. The superradiant beam laser. The atomic beam is generated from an effusive source, like a commercial effusion cell. After emerging from the source (upper right), the atoms are prepared by pumping lasers (blue arrows) in a metastable state prior to entering the cavity (lower left). Inset: The minimal atomic structure needed for the superradiant beam laser to operate. In this three-level scheme, atoms are rapidly prepared in a metastable state $|e\rangle$ by pumping (blue) on a broad transition. Lasing (red) occurs on the long-lived $|g\rangle \leftrightarrow |e\rangle$ transition. Real atomic systems may require more complex pumping schemes.

 © 2020 American Physical Society

The dipole transition frequency ω_a is taken to be near resonant with the frequency ω_c of a single cavity mode, where coupling of the dipoles and cavity is described by the Tavis-Cummings Hamiltonian $\hat{H}(t) = (\hbar g/2)\sum_j \eta[\mathbf{x}_j(t)](\hat{\sigma}_j^+\hat{a} + \hat{a}^\dagger\hat{\sigma}_j^-)$. Here, the summation runs over all atoms in the beam, $\eta[\mathbf{x}_j(t)]$ is a cavity mode function evaluated at position $\mathbf{x}_j(t)$ of atom j at time t, and g is the vacuum Rabi frequency at a cavity antinode. Furthermore, the atomic dipole raising and lowering operators are $\hat{\sigma}_j^+ = (\hat{\sigma}_j^-)^\dagger = |e\rangle_j\langle g|_j$, where $|g\rangle$ and $|e\rangle$ are the atomic ground and excited states, respectively, and the photon annihilation and creation operators of the cavity field mode are $\hat{a}$ and $\hat{a}^\dagger$. Besides this Hamiltonian that couples the atoms and cavity, our model includes photon loss through a cavity mirror with rate κ.

We consider the bad cavity regime, which occurs when κ is much larger than the transit time broadening $1/\tau$, the collective coupling $\sqrt{N}g$, and the Doppler width $\delta_D = k\Delta v_z$. Here $k = 2\pi/\lambda$, λ is the optical wavelength, and Δv_z is the single-atom velocity width along the cavity axis. In this regime, the light field is rigidly anchored to the collective atomic dipole, so that the cavity degrees of freedom can be adiabatically eliminated as $\hat{a} \approx -ig\hat{J}^-/\kappa$. The operator $\hat{J}^- = \sum_j \eta(\mathbf{x}_j)\hat{\sigma}_j^-$ is the collective dipole, which is the sum of the individual atomic dipoles interacting with the cavity mode. New atomic dipoles entering the cavity synchronize with the existing collective dipole due to the atom-cavity interaction [24]. Since there is a large number of atoms in the cavity mode, the true operator equations are well approximated by stochastic differential equations for their complex amplitude equivalents [25];

$$\frac{ds_j^x}{dt} = \frac{\Gamma_c}{2}\eta_j\left[\mathcal{J}^x s_j^z - \eta_j s_j^x(s_j^z+1)\right] - \sqrt{\Gamma_c}\eta_j s_j^z \xi^p, \quad (1)$$

$$\frac{ds_j^y}{dt} = \frac{\Gamma_c}{2}\eta_j\left[\mathcal{J}^y s_j^z - \eta_j s_j^y(s_j^z+1)\right] + \sqrt{\Gamma_c}\eta_j s_j^z \xi^q, \quad (2)$$

$$\frac{ds_j^z}{dt} = -\frac{\Gamma_c}{2}\eta_j\left\{\mathcal{J}^x s_j^x + \mathcal{J}^y s_j^y - \eta_j\left[(s_j^x)^2 + (s_j^y)^2\right]\right\} - \Gamma_c\eta_j^2(s_j^z+1) + \sqrt{\Gamma_c}\eta_j(s_j^x\xi^p - s_j^y\xi^q). \quad (3)$$

Here s_j^x, s_j^y, and s_j^z are the c-number pseudospin variables that correspond to $\hat{\sigma}_j^x = \hat{\sigma}_j^- + \hat{\sigma}_j^+$, $\hat{\sigma}_j^y = i(\hat{\sigma}_j^- - \hat{\sigma}_j^+)$, and $\hat{\sigma}_j^z = \hat{\sigma}_j^+\hat{\sigma}_j^- - \hat{\sigma}_j^-\hat{\sigma}_j^+$. Similarly, $\mathcal{J}^x$ and $\mathcal{J}^y$ represent the operators $\hat{J}^x = \hat{J}^- + \hat{J}^+$ and $\hat{J}^y = i(\hat{J}^- - \hat{J}^+)$. We have defined $\Gamma_c = \mathcal{C}\gamma$, where $\mathcal{C} = g^2/(\kappa\gamma)$ is the cavity cooperativity and γ is the free-space spontaneous emission rate. We use the shorthand $\eta_j = \eta[\mathbf{x}_j(t)]$ and model the cavity mode by $\eta(\mathbf{x}) = [\Theta(x+w) - \Theta(x-w)]\cos(kz)$, where $\Theta(x)$ is the Heaviside step function and w is the cavity beam waist. Spontaneous emission into free space is neglected in Eqs. (1)–(3) because the collective lifetime is much shorter than the spontaneous lifetime [13,24,33,34]. Along the cavity axis, the atoms are randomly assigned a velocity drawn from a Maxwell-Boltzmann distribution at a given temperature. Cavity shot noise is denoted by the stochastic noise variables ξ^q and ξ^p, which have zero mean and are delta correlated as $\langle\xi^a(t)\xi^b(t')\rangle = \delta_{ab}\delta(t-t')$, $a, b \in \{q, p\}$. Each atom enters the cavity with $s_j^z = 1$, and projection noise is included by choosing random (and independent) values $+1$ or -1 for s_j^x and s_j^y [25,35].

Typically, resonance widths in hot gases of atoms are dominated by Doppler and transit time broadening. Although our system is based on a hot gas, these broadening mechanisms vanish when the collective linewidth $N\Gamma_c$ is much greater than δ_D and $1/\tau$. The collective linewidth $N\Gamma_c$ is the rate for an atom to spontaneously emit into the cavity in the presence of other atoms. The principal features of this model can be obtained by dropping the noise terms in Eqs. (1)–(3), corresponding to a mean-field solution that is simple enough to be solved analytically and allows us to classify different phases of emission. The form of the solution for the laser linewidth $\Delta\omega$ is determined by two independent parameters, the first being δ_D and the second being $\Phi\tau^2\Gamma_c = \tau/(N\Gamma_c)^{-1}$, which is the number of collective lifetimes that elapse during τ. In general, we observe a phase transition from broad linewidth emission to superradiant emission with an ultranarrow linewidth [Fig. 2(a)] [25]. Specifically, for large $\delta_D\tau$, the transition threshold is governed by the Doppler width, whereas for small $\delta_D\tau$, transit time broadening determines the regime of superradiant emission. The latter is evident because there is no superradiant emission for $\Phi\tau^2\Gamma_c < 8$ even in the absence of Doppler broadening ($\delta_D\tau \ll 1$). This is because unsynchronized atoms are introduced to the cavity so rapidly that the collective dipole does not establish.

The mean-field analysis predicts an unphysical zero linewidth in the superradiant regime because it neglects quantum noise. In reality, vacuum fluctuations entering the cavity and quantum fluctuations in the atomic dipole components cause phase diffusion, resulting in a nonvanishing linewidth. To determine this linewidth we simulate Eqs. (1)–(3) with noise terms included for $\Phi\tau^2\Gamma_c = 20$. The mean-field theory and c-number simulations agree outside the superradiant regime, whereas inside the superradiant regime only the c-number simulations predict a nonvanishing linewidth. Here the minimum achievable linewidth is Γ_c [Fig. 2(b) inset], which is much smaller than $1/\tau$, implying that our system is robust against single-atom transit time broadening. In other words, the collective atomic dipole stores the optical phase for much longer than the time any individual atom spends in the cavity.

To see how the minimum linewidth in the superradiant phase varies with δ_D, we run simulations with three Doppler widths [Fig. 2(c)]. For $\delta_D\tau = \pi$, the linewidth can be brought down to several Γ_c, and for $\delta_D\tau = 0.2\pi$, the

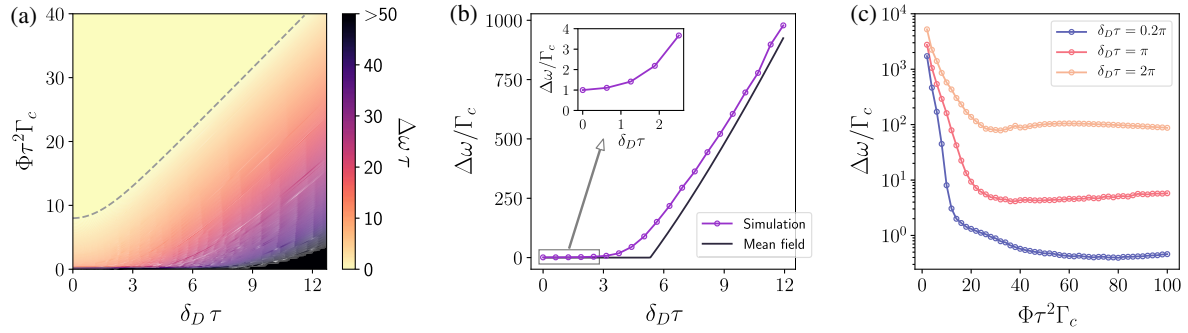

FIG. 2. (a) Mean-field calculations of the linewidth in units of the transit time broadening $1/\tau$, as a function of the Doppler width $\delta_D\tau$ and $\Phi\tau^2\Gamma_c$. Here $\Phi\tau^2\Gamma_c$ is the number of collective lifetimes that elapse during the transit time τ. The black dashed line is the phase transition threshold for steady-state superradiance, above which mean-field calculations predict a zero linewidth. (b) The linewidth in units of Γ_c as a function of the Doppler width for $\Phi\tau^2\Gamma_c = 20$. The markers are simulation results using Eqs. (1)–(3) with $\Phi = 1000/\tau$ and $\Gamma_c = 0.02/\tau$. For every data point, we calculated 100 trajectories each with a simulation time of $T = 2000\tau$. This numerical simulation is compared with the mean-field theory, which is analytic. Inset: Below the phase transition, simulations show an ultranarrow linewidth of order Γ_c, which is 50 times smaller than transit time broadening for these simulation parameters. (c) Simulation results of the linewidth in units of Γ_c as a function of $\Phi\tau^2\Gamma_c$. For every data point, we calculated 100 trajectories each with a simulation time of $T = 200\tau$ and $\Phi = 500/\tau$.

linewidth is Γ_c. These numbers elucidate that narrow-linewidth superradiant emission occurs when the atoms are flying through the cavity so quickly that they move less than $\lambda/2$ along the cavity axis during τ.

To understand the scale of these quantities, we evaluate numerical values for the $^3P_1 \rightarrow {}^1S_0$, $\gamma = 2\pi \times 400$ Hz transition in ^{40}Ca. We take the velocity in the x direction to be that of Ca atoms from an effusion cell operating at ~800 °C. We also consider the case where $\Phi \sim 10^{14}$ atoms/s and the atomic beam is laser cooled in the transverse direction to $\Delta v_z \simeq 0.41$ m/s, corresponding to the $\delta_D\tau = \pi$ curve in Fig. 2(c). Considering a simple cavity with straightforward dimensions (a finesse of 20, a cavity length of 3 cm, and beam waist $w = 300$ μm), we calculated a minimum linewidth of order 10 mHz [25], competitive with the best stable lasers to date [36]. A similar analysis based on the ^{88}Sr intercombination transition yields a minimum linewidth of order 100 mHz [25]. Therefore, ultracoherent light can be extracted from a hot atomic beam with a significant Doppler width, which implies that ultracold atoms may not be required to achieve narrow linewidth superradiant laser emission.

We now turn our attention to the laser output power P. While individual atoms would rarely emit into the cavity mode during their passage, the emission rate is greatly enhanced by collective effects. This enhanced rate leads to a N^2 power scaling [13,25,34], which is a principal feature of superradiant emission. Determining P from both the mean-field and c-number simulation approaches, we find good agreement between the two when $\delta_D\tau$ is comparable to (or below) 0.2π (Fig. 3). For Doppler widths in this regime and for $\Phi\tau^2\Gamma_c = 2\pi^2 \approx 20$, P achieves its maximum value of $0.7\hbar\omega\Phi$, where ω is the center frequency of the output field. Physically this corresponds to each atom emitting an average of 0.7 photons into the cavity mode. Furthermore, we find that the emitted light is second-order coherent by calculating $g^{(2)}(0) \approx 1$ (as shown in the Supplemental Material [25]). Together, Fig. 2(c) and Fig. 3 show that the maximum power and a linewidth of order Γ_c can be simultaneously achieved when $\Phi\tau^2\Gamma_c \approx 20$ and $\delta_D\tau \lesssim 0.2\pi$.

For the ^{40}Ca example mentioned above, we find that $P \approx 0.1$ mW at a linewidth of 40 mHz. For ^{88}Sr, $P = 2.5$ μW at a linewidth of 150 mHz. Significantly, these powers should be sufficient for use with standard laser technology. In contrast, the previously considered cold atom version of the superradiant laser has orders of magnitude weaker power, restricting its use to specialized equipment [13]. The power P is greater in the superradiant beam laser because it has the potential for a much larger intracavity atom number than cold atom systems, where particle numbers have been limited by intrinsic inefficiencies in ultracold gas preparation techniques.

In addition to its relatively large output power and insensitivity to Doppler and transit time broadening, this design is robust against environmental noise. This noise causes cavity length fluctuations, which manifest as cavity resonance frequency noise that dominates the linewidths of cavity-stabilized narrow-linewidth lasers [37]. For these lasers, the frequency noise on the laser output field is equal to the environmental noise in the cavity resonance frequency. However, in a superradiant laser, phase information is stored primarily in the atomic medium, which makes the phase rigid against cavity resonance fluctuations; therefore, these fluctuations are written onto the laser output frequency with a strong suppression factor. This factor is the cavity pulling coefficient [14], defined as $\wp = (\omega - \omega_a)/(\omega_c - \omega_a)$, which is the fractional change in the laser frequency when the cavity resonance fluctuates with respect to the atomic transition. Using mean-field

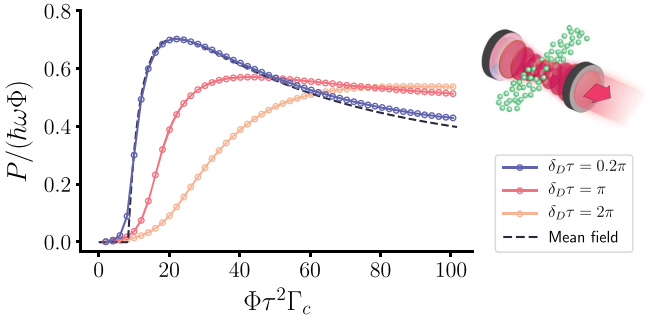

FIG. 3. The output power of the superradiant beam laser. The markers are c-number simulation results. For every data point, we calculated 100 trajectories each with a simulation time of $T = 200\tau$ and $\Phi = 500/\tau$. For $\delta_D\tau = 0.2\pi$, both the mean-field and simulation results peak at $\Phi\tau^2\Gamma_c \approx 20$ with $P = 0.7\hbar\omega\Phi$.

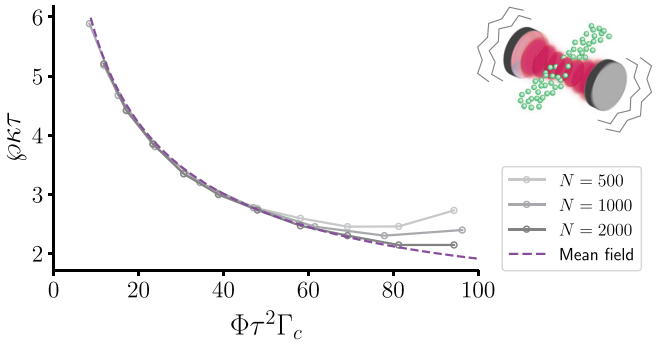

FIG. 4. The cavity pulling coefficient $\wp$ at $\delta_D\tau = 0.2\pi$. A small cavity pulling makes the laser frequency insensitive to environmental noise, such as vibrations. The markers are c-number simulation results with $\kappa = 1000/\tau$ and $\omega_c - \omega_a = 100/\tau$. For every data point, we calculated 100 trajectories each with a simulation time of $T = 100\tau$. As N increases, the simulation results approach the mean-field calculation.

theory, we analytically find that $\wp \propto 1/(\kappa\tau)$, which is the ratio of the cavity photon lifetime to the atom transit time. A value of $\kappa\tau = 1000$ can be achieved with standard optics [25], resulting in $\wp \approx 0.004$ for $\Phi\tau^2\Gamma_c = 20$ (see Fig. 4).

This small $\wp$ makes our design robust against environmental noise sources that limit linewidths of cavity-stabilized lasers. The most common examples are vibration noise [38], thermal Brownian noise [37], and slow drift in the cavity length [25]. The response of cavity resonance frequency to vibration noise is characterized by the acceleration sensitivity K. For the superradiant beam laser, the laser output frequency has an effective acceleration sensitivity $\wp K$. If our design uses a simple V-block cavity with no regard for the vibration isolation found in cutting-edge stable lasers, it would have an acceleration sensitivity of $\wp K \sim 10^{-13}/(\mathrm{m/s^2})$ [25]. Meanwhile, the acceleration sensitivity of the best cavity-stabilized laser to date is of the same order, i.e., $K \sim 10^{-13}/(\mathrm{m/s^2})$ [9].

Thermal Brownian noise causes cavity resonance fluctuations that scale as $1/L$, where L is the cavity length. To suppress this effect, stabilization cavities have been made as long as half a meter [39]. For the superradiant beam laser, the amplitude of thermal noise behaves according to the effective cavity length $L/\wp$. This means that the output frequency of a beam laser based on a compact $L = 3$ cm cavity has the thermal noise of a 7.5 m cavity. Furthermore, slow thermal drift is a practical challenge for cavity-stabilized lasers. The superradiant beam laser has an effective coefficient of thermal expansion (CTE) of $\wp\alpha$, where α is the CTE of the bare cavity. This means that a beam laser based on Invar (an inexpensive and easy-to-machine material) with modest temperature control would have a drift rate similar to that of an ultrastable cavity based on highly temperature-stabilized ultralow expansion glass [25].

Our model is intended to be a simple and clear treatment that correctly reproduces the laser's essential features. This framework allows for an analytically tractable mean-field theory. A more realistic approach would include atom number fluctuations, a Gaussian cavity mode profile, and a distribution of atomic velocities in the x direction. We have numerically confirmed that these effects do not significantly modify the minimum linewidth, maximum power, and minimum pulling coefficient in the superradiant regime.

To realize a superradiant beam laser, one must choose the beam flux, effusive oven design, and cavity parameters to ensure $\Phi\tau^2\Gamma_c > 8$ and $\delta_D\tau < \pi$. For very narrow linewidths, it may be necessary to reduce δ_D by transverse laser cooling the atomic beam. Furthermore, to realize a given linewidth, cavity pulling must be kept small enough to prevent excessive broadening from environmental noise. If cavity pulling remains minuscule, the linewidth can be narrowed by decreasing the cavity finesse and increasing Φ; however, the trade-off is that in the limit of extremely small cavity finesse, the laser power vanishes as atoms radiate appreciably into other modes. We note that if the atomic beam is aggressively cooled such that δ_D is comparable to the recoil frequency, then optomechanical effects are required to model the beam laser correctly [40].

Superradiant lasers based on cold atoms have achieved impressive results, but parasitic heating from atomic repumping has so far limited these systems to pulsed operation [17]. The beam laser design avoids the heating problem since pumping is performed outside the cavity (Fig. 1). Therefore, the beam laser configuration may be a more promising approach for realizing a CW superradiant laser. Furthermore, our design could conceivably be made simpler and less fragile than cold-atom or cavity-stabilized systems. For this reason, the superradiant beam laser may be well suited to operate in accelerating frames, making this design potentially useful for space technology, inertial sensors, geodesy, field-based magnetometry, and astrophysical measurements. We hope that our design will make ultracoherent lasers, which are currently limited to a handful of specialized labs, ubiquitous in quantum science.

We would like to thank J. Bartolotta, J. Cooper, and J. K. Thompson for useful discussions. This research is supported by the Research Centres of Excellence program supported by the National Research Foundation (NRF) Singapore; the Ministry of Education, Singapore; the NSF AMO Grant No. 1806827; NSF PFC Grant No. 1734006; and the DARPA and ARO Grant No. W911NF-16-1-0576. M. H. acknowledges support from a Visiting Fellowship from the University of Pisa, Italy.

*Corresponding author.
nicholson@nus.edu.sg

[1] W. F. McGrew, X. Zhang, R. J. Fasano, S. A. Schäffer, K. Beloy, D. Nicolodi, R. C. Brown, N. Hinkley, G. Milani, M. Schioppo, T. H. Yoon, and A. D. Ludlow, Atomic clock performance enabling geodesy below the centimetre level, Nature (London) **564**, 87 (2018).

[2] S. M. Brewer, J.-S. Chen, A. M. Hankin, E. R. Clements, C. W. Chou, D. J. Wineland, D. B. Hume, and D. R. Leibrandt, $^{27}Al^{+}$ Quantum-Logic Clock with a Systematic Uncertainty Below 10^{-18}, Phys. Rev. Lett. **123**, 033201 (2019).

[3] N. Huntemann, B. Lipphardt, C. Tamm, V. Gerginov, S. Weyers, and E. Peik, Improved Limit on a Temporal Variation of m_p/m_e from Comparisons of Yb^{+} and Cs Atomic Clocks, Phys. Rev. Lett. **113**, 210802 (2014).

[4] R. M. Godun, P. B. R. Nisbet-Jones, J. M. Jones, S. A. King, L. A. M. Johnson, H. S. Margolis, K. Szymaniec, S. N. Lea, K. Bongs, and P. Gill, Frequency Ratio of Two Optical Clock Transitions in $^{171}Yb^{+}$ and Constraints on the Time Variation of Fundamental Constants, Phys. Rev. Lett. **113**, 210801 (2014).

[5] C. Sanner, N. Huntemann, R. Lange, C. Tamm, E. Peik, M. S. Safronova, and S. G. Porsev, Optical clock comparison for Lorentz symmetry testing, Nature (London) **567**, 204 (2019).

[6] S. Kolkowitz, I. Pikovski, N. Langellier, M. D. Lukin, R. L. Walsworth, and J. Ye, Gravitational wave detection with optical lattice atomic clocks, Phys. Rev. D **94**, 124043 (2016).

[7] P. Wcisło, P. Ablewski, K. Beloy, S. Bilicki, M. Bober, R. Brown, R. Fasano, R. Ciuryło, H. Hachisu, T. Ido, J. Lodewyck, A. Ludlow, W. McGrew, P. Morzyński, D. Nicolodi, M. Schioppo, M. Sekido, R. Le Targat, P. Wolf, X. Zhang, B. Zjawin, and M. Zawada, New bounds on dark matter coupling from a global network of optical atomic clocks, Sci. Adv. **4**, eaau4869 (2018).

[8] J. L. Hall, M. S. Taubman, and J. Ye, Laser stabilization, in *Handbook of Optics*, Vol. IV (McGraw-Hill Professional, New York, NY, 2010), Chap. 27, pp. 27.1–27.24.

[9] J. M. Robinson, E. Oelker, W. R. Milner, W. Zhang, T. Legero, D. G. Matei, F. Riehle, U. Sterr, and J. Ye, Crystalline optical cavity at 4 K with thermal-noise-limited instability and ultralow drift, Optica **6**, 240 (2019).

[10] T. A. Ely, E. A. Burt, J. D. Prestage, J. M. Seubert, and R. L. Tjoelker, Using the deep space atomic clock for navigation and science, IEEE Trans. Ultrason. Ferroelectr. Freq. Control **65**, 950 (2018).

[11] R. Bondarescu, A. Schärer, A. Lundgren, G. Hetényi, N. Houlié, P. Jetzer, and M. Bondarescu, Ground-based optical atomic clocks as a tool to monitor vertical surface motion, Geophys. J. Int. **202**, 1770 (2015).

[12] J. Chen, Active optical clock, Chin. Sci. Bull. **54**, 348 (2009).

[13] D. Meiser, J. Ye, D. R. Carlson, and M. J. Holland, Prospects for a Millihertz-Linewidth Laser, Phys. Rev. Lett. **102**, 163601 (2009).

[14] J. G. Bohnet, Z. Chen, J. M. Weiner, D. Meiser, M. J. Holland, and J. K. Thompson, A steady-state superradiant laser with less than one intracavity photon, Nature (London) **484**, 78 (2012).

[15] T. Maier, S. Kraemer, L. Ostermann, and H. Ritsch, A superradiant clock laser on a magic wavelength optical lattice, Opt. Express **22**, 13269 (2014).

[16] A. Roth and K. Hammerer, Synchronization of active atomic clocks via quantum and classical channels, Phys. Rev. A **94**, 043841 (2016).

[17] M. A. Norcia and J. K. Thompson, Cold-Strontium Laser in the Superradiant Crossover Regime, Phys. Rev. X **6**, 011025 (2016).

[18] M. A. Norcia, M. N. Winchester, J. R. K. Cline, and J. K. Thompson, Superradiance on the millihertz linewidth strontium clock transition, Sci. Adv. **2**, e1601231 (2016).

[19] T. Laske, H. Winter, and A. Hemmerich, Pulse Delay Time Statistics in a Superradiant Laser with Calcium Atoms, Phys. Rev. Lett. **123**, 103601 (2019).

[20] C. Hotter, D. Plankensteiner, L. Ostermann, and H. Ritsch, Superradiant cooling, trapping, and lasing of dipole-interacting clock atoms, Opt. Express **27**, 31193 (2019).

[21] S. A. Schäffer, M. Tang, M. R. Henriksen, A. A. Jørgensen, B. T. R. Christensen, and J. W. Thomsen, Lasing on a narrow transition in a cold thermal strontium ensemble, Phys. Rev. A **101**, 013819 (2020).

[22] J. Olson, R. W. Fox, T. M. Fortier, T. F. Sheerin, R. C. Brown, H. Leopardi, R. E. Stoner, C. W. Oates, and A. D. Ludlow, Ramsey-Bordé Matter-Wave Interferometry for Laser Frequency Stabilization at 10^{-16} Frequency Instability and Below, Phys. Rev. Lett. **123**, 073202 (2019).

[23] M. Takamoto, I. Ushijima, N. Ohmae, T. Yahagi, K. Kokado, H. Shinkai, and H. Katori, Test of general relativity by a pair of transportable optical lattice clocks, Nat. Photonics **14**, 411 (2020).

[24] M. Xu, D. A. Tieri, E. C. Fine, J. K. Thompson, and M. J. Holland, Synchronization of Two Ensembles of Atoms, Phys. Rev. Lett. **113**, 154101 (2014).

[25] See Supplemental Material at http://link.aps.org/supplemental/10.1103/PhysRevLett.125.253602 for further details about the theory, the numerics, and the system design, which includes Refs. [26–32].

[26] C. W. Gardiner and M. J. Collett, Input and output in damped quantum systems: Quantum stochastic differential equations and the master equation, Phys. Rev. A **31**, 3761 (1985).

[27] D. A. Tieri, Open quantum systems with applications to precision measurements, Ph.D. Thesis, University of Colorado Boulder, 2015.

[28] M. Abramowitz and I. A. Stegun, *Handbook of Mathematical Functions* (Dover, New York, 1968).

[29] G. D. Domenico, S. Schilt, and P. Thomann, Simple approach to the relation between laser frequency noise and laser line shape, Appl. Opt. **49**, 4801 (2010).

[30] F. Riehle, *Frequency Standards: Basics and Applications* (Wiley-VCH, New York, 2003).

[31] L. Chen, J. L. Hall, J. Ye, T. Yang, E. Zang, and T. Li, Vibration-induced elastic deformation of Fabry-Perot cavities, Phys. Rev. A **74**, 053801 (2006).

[32] T. Legero, T. Kessler, and U. Sterr, Tuning the thermal expansion properties of optical reference cavities with fused silica mirrors, J. Opt. Soc. Am. B **27**, 914 (2010).

[33] The conditions for neglecting free space spontaneous emission are that $N\Gamma_c \gg \gamma$ and $\gamma\tau \ll 1$. We simulated this system with free space spontaneous emission and confirmed that our model (which neglects this effect) reproduces the correct minimum $\Delta\omega$, maximum P, and minimum $\wp$.

[34] D. Meiser and M. J. Holland, Steady-state superradiance with alkaline-earth-metal atoms, Phys. Rev. A **81**, 033847 (2010).

[35] J. Schachenmayer, A. Pikovski, and A. M. Rey, Many-Body Quantum Spin Dynamics with Monte Carlo Trajectories on a Discrete Phase Space, Phys. Rev. X **5**, 011022 (2015).

[36] W. R. Milner, J. M. Robinson, C. J. Kennedy, T. Bothwell, D. Kedar, D. G. Matei, T. Legero, U. Sterr, F. Riehle, H. Leopardi, T. M. Fortier, J. A. Sherman, J. Levine, J. Yao, J. Ye, and E. Oelker, Demonstration of a Timescale Based on a Stable Optical Carrier, Phys. Rev. Lett. **123**, 173201 (2019).

[37] M. J. Martin and J. Ye, High-precision laser stabilization via optical cavities, in *Optical Coatings and Thermal Noise in Precision Measurement* (Cambridge University Press, Cambridge, England, 2012), p. 237–258.

[38] R. L. Filler, The acceleration sensitivity of quartz crystal oscillators: A review, IEEE Trans. Ultrason. Ferroelectr. Freq. Control **35**, 297 (1988).

[39] S. Häfner, S. Falke, C. Grebing, S. Vogt, T. Legero, M. Merimaa, C. Lisdat, and U. Sterr, 8×10^{-17} fractional laser frequency instability with a long room-temperature cavity, Opt. Lett. **40**, 2112 (2015).

[40] S. B. Jäger, J. Cooper, M. J. Holland, and G. Morigi, Dynamical Phase Transitions to Optomechanical Superradiance, Phys. Rev. Lett. **123**, 053601 (2019).